**ORIGINAL RESEARCH** **Open access**

# Predicting Energy Savings of Façade Alternatives Using Deep Neural Networks in Early Building Design

Daniel Green[1*], Olivia Walker[1], Thomas Bell[2]

## Abstract

Securing high-efficiency building facade systems is a cornerstone of improving overall building energy performance. This task, however, hinges considerably on determinations made during the preliminary design stage, which becomes enormously complicated when one considers the sheer volume of design variables and the ambiguities typical of early-phase development. The present study investigates whether deep learning networks can serve as reliable tools for approximating the energy savings associated with distinct facade alternatives during the conceptual building design phase. EnergyPlus™ was used to run building energy simulations that capture the energy behavior of two contrasting facade solutions—Ultra-High-Performance Fiber-Reinforced-Concrete and conventional panel systems—across a range of operational scenarios. The simulation outputs, derived from 14 buildings distributed across 14 geographic locations, were used to train 3 separate deep learning networks, each dedicated to projecting heating, cooling, and total site energy savings. The predictive fidelity of these deep networks was subsequently compared against that of three established data-driven modeling techniques: Gradient Boosting Machines, Random Forest, and Generalized Linear Regression. The findings indicated that the deep learning network formulated for total site energy savings projections surpassed all competing models, posting a mean absolute error of 1.59 and a root mean square error of 3.48, with Gradient Boosting Machines ranking second, Random Forest third, and Generalized Linear Regression placing last. In parallel, the deep networks tasked with predicting cooling and heating energy savings achieved the lowest mean average errors of 0.20 and 1.17, respectively, among all modeling approaches. It is envisioned that a decision-support platform built on this methodological framework will enable architects and design professionals to quantify energy savings across facade alternatives at the earliest stages of design deliberation.

**Keywords** Deep learning, Early-stage building facade design, Building energy savings estimation, Deep neural networks

*Correspondence:
Daniel Green
daniel.green@unsw.edu.au
[1] Department of AI for Smart Grid Resilience, Faculty of Engineering, University of New South Wales, Sydney, Australia
[2] Department of Intelligent Energy Systems, Faculty of Engineering, University of Melbourne, Melbourne, Australia

## Introduction

Spiraling energy expenditures and the intensifying threat of climate change have brought into sharp relief the imperative to strengthen energy-efficiency provisions in buildings, which together account for a sizable share—on the order of 20 percent—of worldwide energy demand [1]. Within the United States alone, the combined consumption of residential and commercial structures reached 21 quadrillion British thermal units (Btu) in 2019, accounting for 28% of the nation's aggregate end-use energy consumption that year [2]. Even incremental gains in the energy performance of buildings can translate into meaningful reductions in energy use and pollutant emissions. Pursuing energy-efficiency upgrades across

This is an open access article distributed under the terms of the Creative Commons Attribution-NonCommercial-ShareAlike 4.0 International License (CC BY-NC-SA 4.0), which permits non-commercial use, distribution, reproduction, and adaptation in any medium or format, provided that appropriate credit is given to the original author(s) and source, a link to the license is provided, and any changes made are indicated. Adapted material must be distributed under the same license.

© 2026 The Author(s). | Published by Institute of Smart Energy Systems Press

the building construction industry represents a direct yet potent avenue for reducing energy requirements, operational costs, and total life-cycle expenditures [3].

The earliest moments of a building's design trajectory offer the most impactful opportunities for embedding energy-conscious strategies [4]. The resolutions formed during this formative phase carry outsized weight in shaping ultimate building performance, often dictating whether the entire design endeavor meets its objectives or falls short [5]. Facade assemblies play a central role in mediating a structure's thermal dynamics, as they constitute the physical division between conditioned interior volumes and the ambient exterior, managing bidirectional heat exchange across that threshold [6]. For this reason, committing to an energy-efficient facade solution at the very outset of design can dramatically improve building energy performance and bolster broader sustainability goals. A widely adopted tactic for weighing the merits of competing facade proposals entails running building energy simulations (BESs) to characterize the projected energy footprint of each candidate system [7]. Yet for all their precision, BPS platforms presuppose access to richly detailed building models that are customarily unavailable until the design process has advanced considerably [8].

The maturation of Artificial Intelligence (AI) technologies has now brought them to a point where they furnish tangible, practical returns across a broad spectrum of use cases [9]. One area of particular promise lies in building data analytics, where AI-driven insights can inform actionable strategies for building energy stewardship. Within the building engineering research community, forecasting building energy consumption has emerged as a premier application of AI, with energy use intensity serving as a standard yardstick for gauging efficiency performance [10]. Accordingly, the capacity to anticipate energy savings through AI-enabled methodologies can profoundly influence the comparative evaluation of building design pathways.

A growing body of contemporary scholarship has been directed at crafting machine learning and data mining algorithms capable of projecting building energy utilization. These computational approaches are adept at teasing out latent regularities, structural patterns, and complex non-linear couplings embedded within building datasets, thereby yielding predictions of impressive accuracy. Rule-based machine learning frameworks, as one illustration, can distill fundamental operational logics from energy consumption records and recast them into prescriptive, energy-conserving directives. Ashouri *et al*. [11] leveraged this strategy to isolate distinct behavioral occupancy routines that contribute to lower building energy demand. Similarly, Abediniangerabi *et al.* [8] applied rule-based association mining techniques to develop guidance for energy-saving substitutions of traditional facade assemblies with novel facade technologies.

A separate strand of inquiry evaluates design permutations by estimating the energy footprint of buildings configured under different specifications. Predictive paradigms spanning generalized linear models, tree-structured models, and artificial neural networks have been applied to this challenge in the existing literature. Linear regression formulations, representing the most parsimonious class of machine learning tools, are often characterized as white-box methods on account of their transparency, operational simplicity, and the intuitive grasp they afford modelers [12]. Multiple research teams have deployed diverse linear regression variants to project building energy metrics. Amiri *et al.* [3], for example, applied multivariate linear regression to model consumption patterns across US commercial building stock, parameterizing their model in terms of envelope attributes and occupancy scheduling profiles. In a separate contribution, Zeng *et al.* [13] used Gaussian process regression for electricity consumption forecasting, observing that combining a Gaussian process kernel with a conventional linear regression backbone could markedly accelerate model training—an important consideration for large datasets. Wu *et al.* [14] pursued an analogous analytical pathway to estimate energy consumption indices in mixed-use buildings, calibrating a linear regression framework against streaming monitoring data collected from 30 dedicated-use buildings and 20 mixed-use counterparts. Regression-based approaches confer notable strengths in accessibility, expeditious deployment, and interpretive clarity. Yet they remain fundamentally limited by their inability to accommodate the non-linear input-output mappings that pervade building energy phenomena. Furthermore, constructing an effective linear regression model requires deliberate feature engineering and judicious variable selection to mitigate the adverse effects of multicollinearity among predictor variables [12].

© 2026 The Author(s). | Published by Institute of Smart Energy Systems Press

Tree-based models represent an additional family of machine learning methods that depend on hierarchical, branching architectures to tackle regression and classification problems [15]. One of their principal strengths lies in their interpretability and transparency, as these models can be visualized graphically, making them straightforward to understand [16]. Although a solitary tree structure tends to be unstable and overly sensitive to perturbations in the training data, blending multiple tree models can produce a powerful ensemble learner that largely circumvents this fragility [17]. A range of tree-based formulations—including Bagging, Random Forest (RF), Gradient Boosting Model (GBM), and Extreme Gradient Boosting (XGBoost)—has been documented in the scholarly literature for projecting building energy demand. By way of illustration, Pham *et al.* [18] harnessed a Random Forest prediction framework to generate short-term, hourly-resolution energy consumption estimates for a collection of buildings. Elsewhere, Touzani *et al.* [19] adopted the GBM approach to develop a baseline model of energy consumption intended for quantifying savings, noting that their GBM construction surpassed both a piecewise linear regression specification and a random forest algorithm in predictive accuracy. Tree-based techniques offer several benefits over conventional linear regression. Chief among these is the capacity to model intricate, non-linear relationships among predictor variables [20]. That said, these approaches are not without their shortcomings. An individual decision tree remains inherently volatile when confronted with even minor alterations to the input dataset. Random Forest configurations exact a heavier toll in terms of computational demand and training duration than GBM formulations, whereas GBM models are prone to overfitting. Beyond this, tree-based algorithms are highly complex constructs that require significant investment in training effort, computational resources, and careful calibration of model hyperparameters [21].

Among black-box modeling paradigms, Artificial Neural Networks (ANNs) have achieved the greatest currency for predicting building energy utilization [22]. ANNs are designed to mimic the rudimentary organization of the human brain, drawing inspiration from what are termed processing units [17]. Concretely, a neural network comprises a multitude of elementary yet richly interconnected computational elements, or nodes, called 'neurons,' which are structured into successive layers and which transform incoming information through dynamic, state-driven reactions to external stimuli. What sets ANNs apart from many competing predictive frameworks, including linear regression models, is their intrinsic capacity to perform non-linear analyses on problems of considerable complexity [22, 23]. Melo *et al*. [24] investigated the feasibility of deploying ANNs to improve the fidelity of surrogate models approximating building energy performance, training an ANN to replicate outputs from detailed building simulations. In a related study, Rahman and Smith [25] calibrated an ANN to forecast fuel consumption for a small office, a supermarket, and a restaurant situated across several climate zones. Their systematic comparison, which gauged the predictive accuracy of ANN models against Gaussian process (GP) regression, multivariate linear regression, and ridge regression, demonstrated that ANN models outperformed all alternatives except GP regression. Although ANNs afford greater flexibility in detecting and modeling non-linear interactions within data, they nonetheless require antecedent feature engineering and extraction steps if they are to deliver superior predictive performance. Moreover, simple ANN architectures possess inherently shallow structures, which severely limits their ability to extract informative features directly from raw, unrefined input data [26].

The challenge of estimating the energy savings associated with competing facade design alternatives is an inherently complicated undertaking, as it must factor in a dense fabric of interdependencies and mutual interactions between a building's physical properties and the broader context—encompassing climate, temperature, wind, and related environmental variables—against which the building's performance is being evaluated. Despite the meaningful strides made by earlier research efforts, the body of knowledge still has notable deficiencies in applying deep learning techniques to inform early-stage facade design decisions. The core aim of the present work is to develop deep neural networks (DNNs) that can reliably estimate the heating, cooling, and total site energy savings achieved by buildings with different facade assembly configurations, with the ultimate goal of deploying these networks as a decision-support instrument during the conceptual design phase. To validate the practicality of deep neural networks for estimating energy savings, DNNs were tasked with predicting the heating, cooling, and total site energy savings achieved by an innovative ultra-high-performance fiber-reinforced concrete (UHP-FRC) facade system, which served as the investigative case study. The predictive accuracy of the deep networks was measured against that of a shallow ANN, a linear regression model, a Random Forest model, and a GBM model, with assessments grounded in multiple standard performance metrics, including mean absolute error (MAE) and root mean square error (RMSE). This paper presents, for the first time,

© 2026 The Author(s). | Published by Institute of Smart Energy Systems Press

evidence that DNNs can forecast the energy savings attributable to a range of novel facade systems with a degree of precision that surpasses that achievable by existing data-driven methodologies (e.g., GBM, RF, and GLM) at the early building design stage. The contribution of this research to the state of knowledge lies in the formulation of a data-driven framework to estimate the energy savings delivered by different building facade assembly designs at the earliest stages of the design process.

# Materials and Methods

**Figure 1** outlines the methodological workflow adopted in this research. The overall framework is structured around three principal phases: 1) the construction of a database cataloging the energy savings of the UHP-FRC facade system relative to a baseline facade system across a defined set of simulation scenarios using BPSs; 2) the execution of descriptive statistical analyses on the assembled dataset; 3) the design and training of predictive models rooted in deep neural network architectures; and 4) the evaluation of the trained models' predictive capabilities and the comparison of their performance against widely utilized predictive models (namely, shallow ANNs, Gradient Boosting Machines, Random Forest, and Generalized Linear Regression). These three thematic components are elaborated in greater depth in the following subsections.

© 2026 The Author(s). | Published by Institute of Smart Energy Systems Press

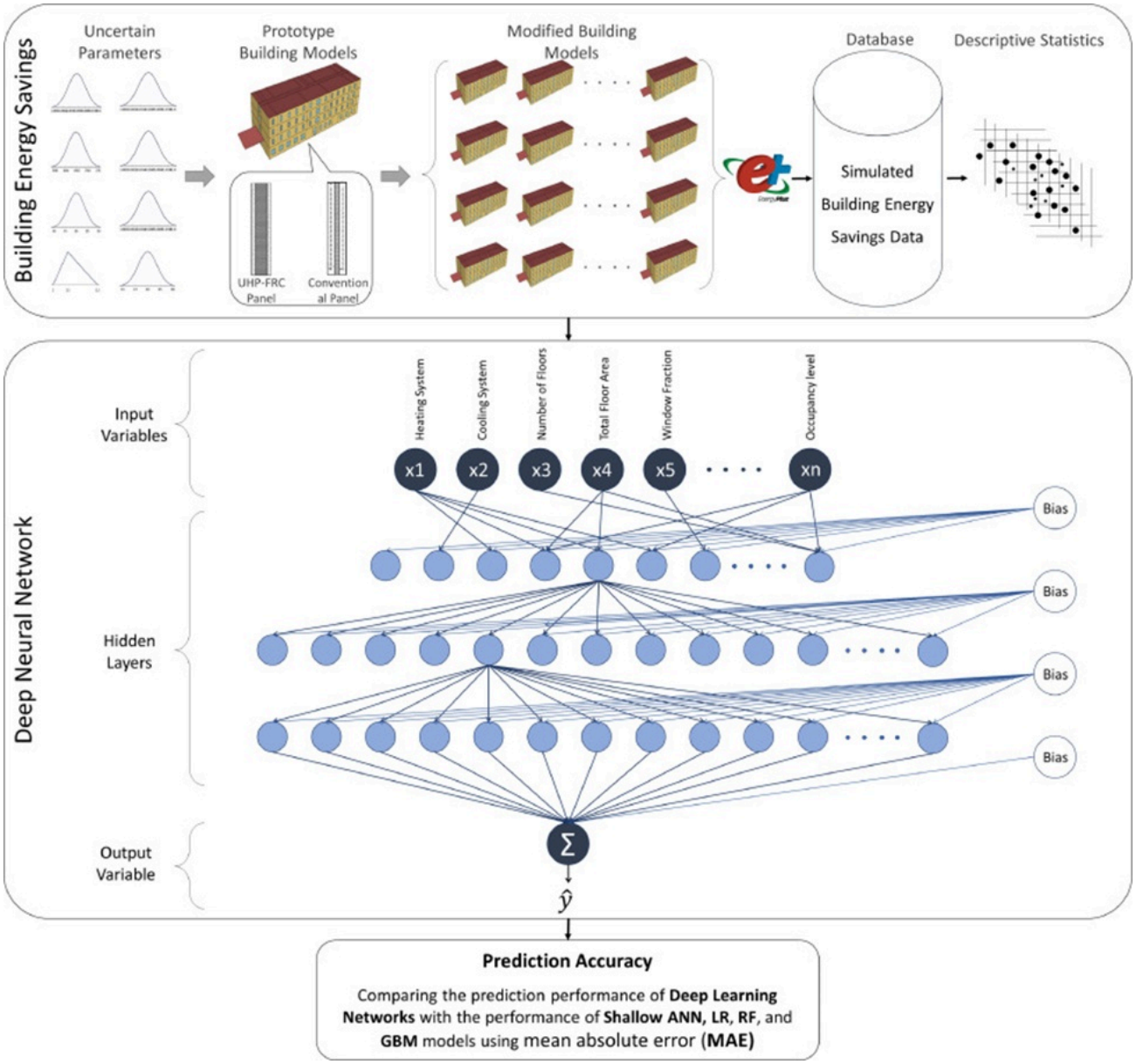



**Figure 1.** Proposed methodology.

## Database development

BPS tools were deployed to conduct building energy simulations to quantify the energy performance of buildings incorporating the two rival facade systems. **Figure 2** illustrates the physical configurations of the UHP-FRC panel and the conventional facade panel [26-29] adopted as the comparative case study in this work. The simulation campaign spanned a wide array of scenarios (covering variations in building typology and climatic settings) and explicitly accounted for uncertainty. Thirteen prototype building models issued by the DOE [30]—encompassing high-rise and mid-rise apartment blocks, a large hotel, a small hotel, a primary school, a secondary school, a fast-food restaurant, a strip mall, a standalone retail store, a warehouse, a small office, a mid-size office, a large office, and a hospital—were chosen to represent the heterogeneity of building contexts examined in this study. These archetypal buildings are commercial reference models endorsed by the Department of Energy (DOE) and were developed in accordance with

© 2026 The Author(s). | Published by Institute of Smart Energy Systems Press

ANSI/ASHRAE/IES Standard 90.1 [30]. Taken together, these models account for 75% of the total commercial building floor area found across the United States. Within each model, the exterior wall assemblies were replaced with the two competing facade panel systems. In addition, 15 representative locations distributed throughout the US (covering the full spectrum of DOE climate zone classifications) were selected for the building energy simulation runs to ensure that the effects of diverse meteorological regimes were adequately represented in the analysis **(Figure 3).**

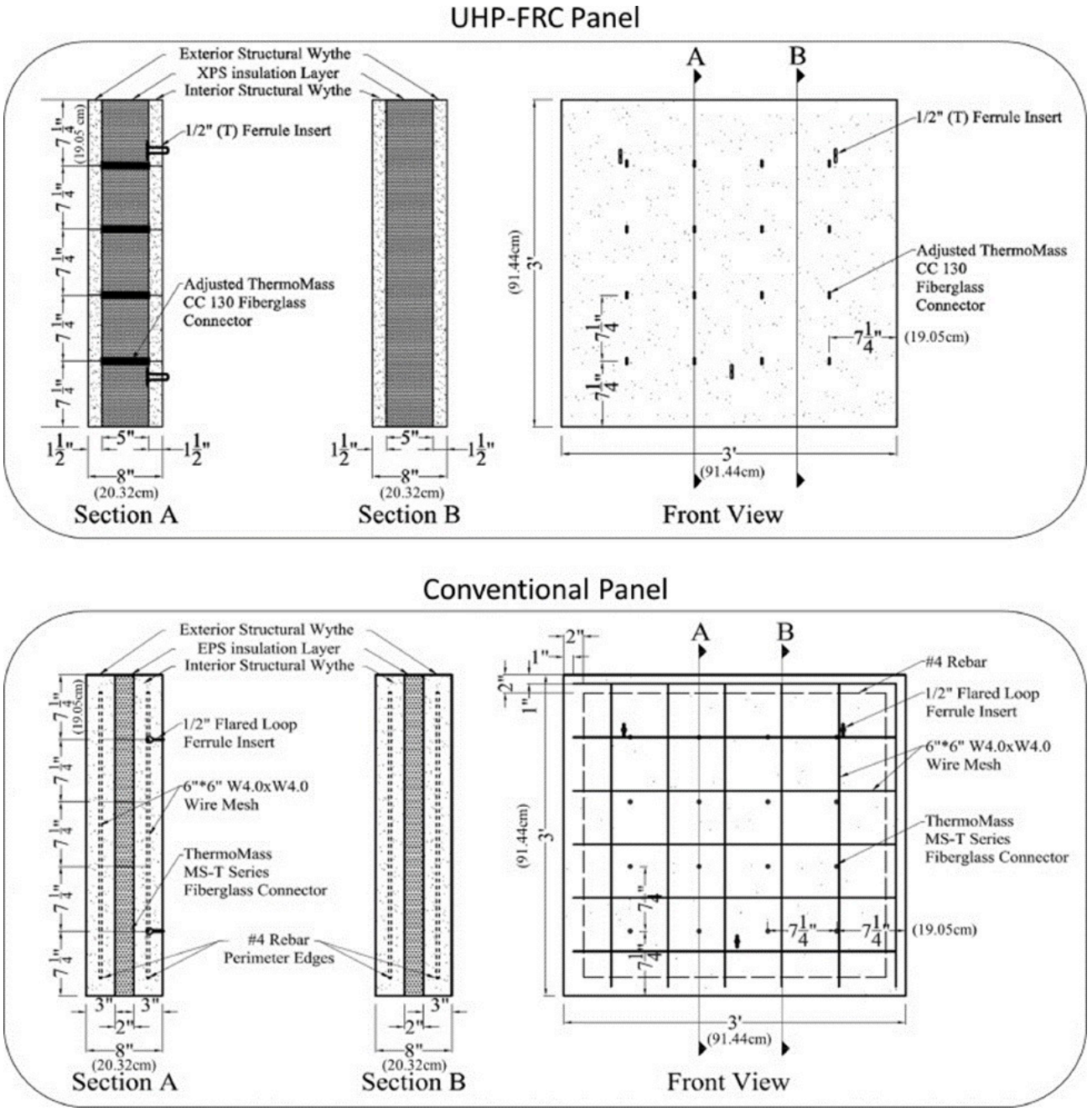



**Figure 2.** Front and section views of Conventional and UHP-FRC panel assemblies [31].

© 2026 The Author(s). | Published by Institute of Smart Energy Systems Press

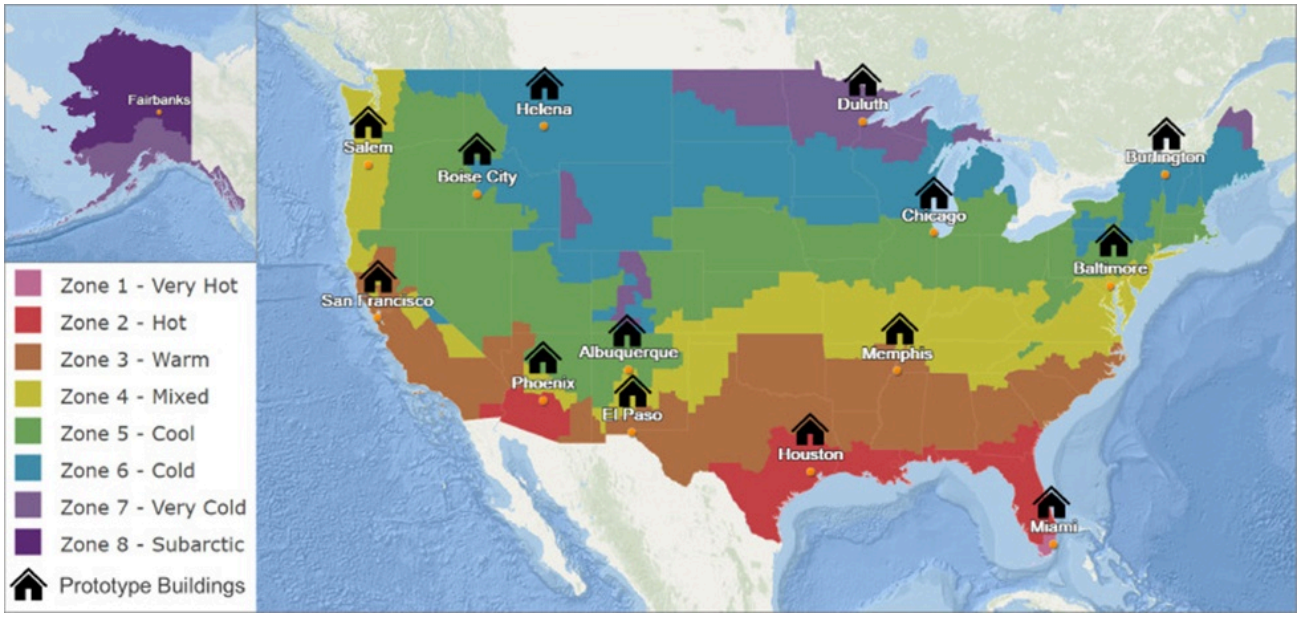



**Figure 3.** DOE climate zones and representative cities [30].

The existing body of research has repeatedly stressed the need to treat key inputs as uncertain in building energy simulations to better align computational estimates with measured energy consumption [32]. Following this guidance, three primary sources of uncertainty were selected from the literature and deliberately incorporated into the simulation protocol. These comprised the rate of air infiltration [33], the intensity of occupancy [34], and the magnitude of lighting loads [35]. Beyond these operational factors, six thermophysical properties characterizing the facade materials—concrete thermal conductivity, concrete specific heat, concrete density, insulation density, insulation thermal conductivity, and insulation specific heat—were likewise handled as stochastic inputs. **Table 1** collates the recommended probability density functions, central tendency values, and standard deviation values for each uncertain parameter, as documented in prior studies. Through Monte Carlo simulation, one hundred random variates were independently drawn for every uncertain parameter in accordance with its prescribed distribution. Taken collectively, these draws generate 100^9 plausible combinations. To render the simulation effort tractable, the Latin hypercube sampling (LHS) technique [36] was employed to obtain 100 stratified samples for each building model. The selection of 100 iterations was deliberate, intended to ensure robust results and fall above the minimum of 80 iterations recommended by Macdonald [37]. The sampled assemblies of randomly generated uncertain parameter values were then seeded into the DOE prototype building models. Afterward, each building model, now hosting its assigned set of uncertain inputs, was processed through the EnergyPlusTM computational engine [38]. Every distinct building representation—incorporating 100 unique amalgamations of the uncertain parameters—underwent simulation in fourteen different geographic localities. In aggregate, this yielded 19,600 individual simulation runs for structures clad with conventional panels and an equivalent number for those clad with UHP-FRC panels. For each scenario, the energy savings attributed to the UHP-FRC panels were quantified as the difference in energy consumption observed after swapping the conventional panel (the reference facade assembly) for the UHP-FRC system.

**Table 1.** Recommended probability distributions, mean values, and standard deviations of uncertain parameters.

| Parameter subject to uncertainty | Unit | Probability distribution | Conventional panel parameters | UHP-FRC panel parameters | Source references |
|---|---|---|---|---|---|
| Thermal conductivity of insulation material | W/m·K | Normal | μ = 0.0058, σ = 0.0023 | μ = 0.0058, σ = 0.0023 | [32, 39-45] |

© 2026 The Author(s). | Published by Institute of Smart Energy Systems Press

| | | | | | |
|---|---|---|---|---|---|
| Specific heat capacity of insulation | J/kg·K | Normal | μ = 645, σ = 38.7 | μ = 645, σ = 38.7 | [32, 39-45] |
| Density of insulation layer | kg/m³ | Normal | μ = 28, σ = 5.3 | μ = 20, σ = 3.78 | [32, 39-45] |
| Thermal conductivity of concrete | W/m·K | Normal | μ = 2.31, σ = 0.13 | μ = 1.77, σ = 0.10 | [32, 39-45] |
| Specific heat capacity of concrete | J/kg·K | Normal | μ = 832, σ = 49.9 | μ = 1010, σ = 60.6 | [32, 39-45] |
| Concrete density | kg/m³ | Normal | μ = 2322, σ = 441 | μ = 2403, σ = 456 | [32, 39-45] |
| Air infiltration rate | l/s·m² | Normal | μ = 1.06, σ = 0.07 | μ = 1.06, σ = 0.07 | [32, 39-45] |
| Occupant density | Person | Triangular | a = 1, c = 2.5, b = 5.2 | a = 1, c = 2.5, b = 5.2 | [32, 39-45] |
| Interior lighting power density | W/m² | Uniform | a = 0.01, b = 5 | a = 0.01, b = 5 | [32, 39-45] |

To construct the analytical database, the physical descriptors of each building model and the associated meteorological variables were harvested from the representative building archetypes and their paired cities within the DOE climate zone framework. By way of example, within a single simulation run, a given building can be delineated by a vector of parameters reflecting its geometric makeup (e.g., gross floor area, story count, aspect ratio, and glazing fraction), its mechanical plant (e.g., heating and cooling system typologies), its functional occupancy (e.g., number of building users), and the ambient weather profile (e.g., annual and monthly extreme, mean, and minimum air temperatures alongside wind speed records). The finalized database comprises 19,600 observations, defined by 39 independent variables—specifically, six building design features, 30 climatic predictors, and three uncertain building parameters—along with three dependent variables that capture the magnitude of heating, cooling, and total site energy savings. A concise inventory of the variables harnessed for predictive model development is presented in **Table 2.**

**Table 2.** Summary of features used for developing predictive models.

| No. | Parameter group | Variable description | Data type | Range/Categories | Measurement unit |
|---|---|---|---|---|---|
| 1 | Building Configuration Variables | Space Heating Technology | Categorical | [Water Heat Pumps, Gas Furnace, PTAC, Air-Source Heat Pump, Gas Boiler] | – |
| 2 | Building Configuration Variables | Space Cooling Technology | Categorical | [Water Heat Pumps, Split System DX, Air-Cooled Chiller, Packaged Air Conditioning, Air Conditioner, Chillers] | – |
| 3 | Building Configuration Variables | Building Height (Floors) | Numerical | [1, 10] | – |
| 4 | Building Configuration Variables | Building Aspect Ratio | Numerical | [1, 5.07] | Ratio |

© 2026 The Author(s). | Published by Institute of Smart Energy Systems Press

| | | | | | |
|---|---|---|---|---|---|
| 5 | Building Configuration Variables | Window-to-Wall Fraction | Numerical | [0.0071, 0.35] | Ratio |
| 6 | Building Configuration Variables | Gross Floor Area | Numerical | [511, 22428] | $m^2$ |
| 7 | Climate Variables | Mean Annual Maximum Temperature | Numerical | [3.5, 30] | °C |
| 8 | Climate Variables | Mean Annual Minimum Temperature | Numerical | [-8, 21] | °C |
| 9 | Climate Variables | Mean Annual Temperature | Numerical | [-2.5, 25] | °C |
| 10 | Climate Variables | January Maximum Temperature | Numerical | [-17, 24] | °C |
| 11 | Climate Variables | February Maximum Temperature | Numerical | [-12, 26] | °C |
| 12 | Climate Variables | March Maximum Temperature | Numerical | [-4, 27] | °C |
| 13 | Climate Variables | April Maximum Temperature | Numerical | [7, 29] | °C |
| 14 | Climate Variables | May Maximum Temperature | Numerical | [16, 35] | °C |
| 15 | Climate Variables | June Maximum Temperature | Numerical | [19, 40] | °C |
| 16 | Climate Variables | July Maximum Temperature | Numerical | [19, 41] | °C |
| 17 | Climate Variables | August Maximum Temperature | Numerical | [19, 40] | °C |
| 18 | Climate Variables | September Maximum Temperature | Numerical | [13, 38] | °C |
| 19 | Climate Variables | October Maximum Temperature | Numerical | [0, 32] | °C |
| 20 | Climate Variables | November Maximum Temperature | Numerical | [-12, 28] | °C |
| 21 | Climate Variables | December Maximum | Numerical | [-15, 26] | °C |

© 2026 The Author(s). | Published by Institute of Smart Energy Systems Press

| | | | | | |
|---|---|---|---|---|---|
| | | Temperature | | | |
| 22 | Climate Variables | January Minimum Temperature | Numerical | [-27, 16] | °C |
| 23 | Climate Variables | February Minimum Temperature | Numerical | [-25, 17] | °C |
| 24 | Climate Variables | March Minimum Temperature | Numerical | [-19, 18] | °C |
| 25 | Climate Variables | April Minimum Temperature | Numerical | [-6, 20] | °C |
| 26 | Climate Variables | May Minimum Temperature | Numerical | [3, 23] | °C |
| 27 | Climate Variables | June Minimum Temperature | Numerical | [9, 26] | °C |
| 28 | Climate Variables | July Minimum Temperature | Numerical | [11, 28] | °C |
| 29 | Climate Variables | August Minimum Temperature | Numerical | [8, 28] | °C |
| 30 | Climate Variables | September Minimum Temperature | Numerical | [2, 25] | °C |
| 31 | Climate Variables | October Minimum Temperature | Numerical | [-8, 23] | °C |
| 32 | Climate Variables | November Minimum Temperature | Numerical | [-21, 20] | °C |
| 33 | Climate Variables | December Minimum Temperature | Numerical | [-25, 17] | °C |
| 34 | Climate Variables | Extreme Wind Velocity (1%) | Numerical | [7.7, 12.8] | m/s |
| 35 | Climate Variables | Extreme Wind Velocity (2.5%) | Numerical | [6.7, 11.5] | m/s |
| 36 | Climate Variables | Extreme Wind Velocity (5%) | Numerical | [5.5, 10.5] | m/s |
| 37 | Building Uncertainty Variables | Lighting Power Density | Numerical | [1, 9] | $W/m^2$ |
| 38 | Building Uncertainty Variables | Occupant Density | Numerical | [1, 5] | Persons per space |

© 2026 The Author(s). | Published by Institute of Smart Energy Systems Press

| | | | | | |
|---|---|---|---|---|---|
| 39 | Building Uncertainty Variables | Air Infiltration Rate | Numerical | [0.000482363, 0.000637798] | $m^3/s \cdot m^2$ |
| 40 | Response Variables | Cooling Energy Savings | Numerical | [-3.1, 4.7] | $MJ/m^2$ |
| 41 | Response Variables | Heating Energy Savings | Numerical | [-30.8, 37.6] | $MJ/m^2$ |
| 42 | Response Variables | Total Site Energy Savings | Numerical | [-29.89, 32.2] | $MJ/m^2$ |

Descriptive statistical methods were applied to summarize the fundamental characteristics of the simulation-derived dataset. The empirical distributions of several salient attributes—among them heating and cooling system categories, gross floor area, and building height in stories—were examined graphically to gauge the degree of variation present. In parallel, both Spearman rank-order and Pearson product-moment correlation analyses were conducted to numerically assess the strength and direction of relationships between the explanatory and response variables.

## Deep neural networks

An artificial neural network (ANN) can be conceptualized as an arrangement of rudimentary functional modules, known as "neurons," that are interconnected through weighted linkages to form an interconnected processing fabric [46]. In operational terms, these artificial neurons mimic the behavior of biological brain cells, which function as the core information-processing elements of the human cognitive apparatus [47, 48]. From a formal mathematical standpoint, a neuron embodies a bounded, non-linear transformation parameterized in the following manner:

$$o = f\left(x_1,\ x_2, \ldots, x_n; w_1,\ \ w_2, \ldots, w_p\right) = f(x, w) \quad (1)$$

Where the term x represents the vector of incoming signals to the neuron, w corresponds to the vector of tunable weights associated with those signals, and f(.) denotes a non-linear activation function.

Training a neural network unfolds across numerous iterative cycles. During each forward propagation, the connection weights are traversed sequentially to compute a predicted output. The discrepancy between this prediction and the known true value, or ground truth, is subsequently quantified as a prediction error. The back-propagation procedure then determines the necessary corrections to the weights that would reduce this error. This iterative forward-and-backward sequence is repeated throughout the training regimen, allowing the network to gradually internalize the latent input-output mapping present in the training exemplars. After training concludes, the network stands ready to generate forecasts for input patterns it has never previously encountered [46].

Deep neural networks represent a hierarchical extension of shallow architectures, distinguished by the incorporation of multiple hidden processing strata. Owing to this depth, deep networks can assemble progressively richer, multi-tiered representations of the input data, thereby elevating modeling fidelity while rendering manual feature extraction unnecessary [49]. **Figure 4** juxtaposes the topological layouts of a deep network and a shallow network. As the illustration shows, both network variants share a common tripartite organization: an input layer, one or more hidden layers, and a terminal output layer. The fundamental structural divergence lies in the number of hidden layers: a shallow network is restricted to a single such layer, whereas a deep network incorporates two or more. The presence of multiple hidden

© 2026 The Author(s). | Published by Institute of Smart Energy Systems Press

layers equips the deep architecture to disentangle substantially more complex interdependencies and higher-order patterns operating among the manifold factors that govern building energy consumption.

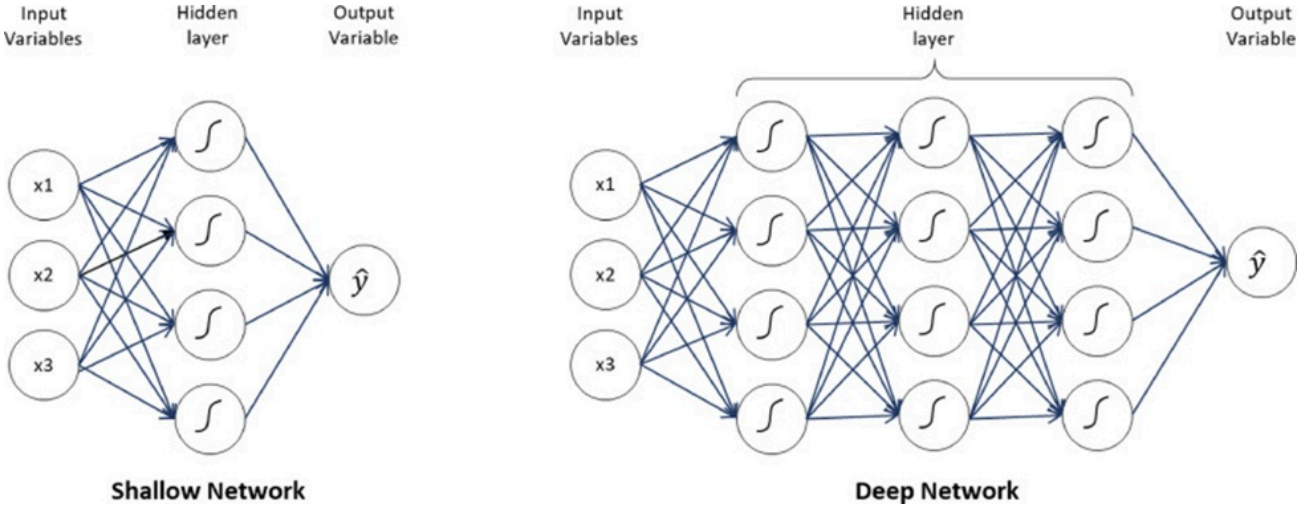



**Figure 4.** Shallow and deep neural network structures.

## Modeling approach

Training was conducted on three independent, sequentially constructed deep neural networks, each tasked with projecting building energy savings. Drawing on the Pareto principle, the conventional practice for partitioning datasets assigns 80% of the records to the training subset and 20% to the test subset [50]. Owing to the comparatively large volume of the simulation dataset, which holds 19,600 data points, a more aggressive 90/10 division was implemented to yield a model with enhanced generalization capacity. Under this scheme, 90% of the simulated energy-savings data fed the training procedure. The consequence of such a split ratio is a potential rise in prediction variance, counterbalanced by a reduction in prediction bias. The remaining one-tenth of the data was reserved exclusively as unseen test data against which the predictive reliability of the fully trained networks was subsequently evaluated. **Table 3** details the structural composition of the deep neural networks developed for this estimation task. A uniform architecture governed all three networks, each built from four fully connected dense layers, populated, respectively, with 100, 50, 20, and a single neuron. Positioned between the initial and second dense layers was a dropout layer with a dropout fraction of 0.1, introduced to provide regularization and mitigate the risk of overfitting. The first dense layer used a hyperbolic tangent (Tanh) activation. Rectified linear unit (ReLU) activations were adopted for the subsequent second and third dense layers. The final layer used its standard linear activation function.

The loss metric guiding the training process was mean squared error, minimized via the NADAM (Nesterov-accelerated adaptive moment) optimizer. To ensure the loss function had sufficient time to plateau, the epoch count was deliberately set to an upper bound of 500. In parallel, an early stopping rule was activated, terminating training at the iteration at which the mean absolute error failed to improve further, thereby averting overfitting. **Figure 5** charts the evolution of the training and testing losses as the iteration count increases. The graphic confirms that, for each network, the loss measure approaches saturation near the 100-iteration mark. As shown, convergence was reached, and training was suspended at iteration 100 for the total building energy savings network, at iteration 120 for the cooling energy savings network, and at iteration 175 for the heating energy savings network. The choice of batch size determines the fidelity of the error gradient approximation during model optimization. Its primary footprint is computational: a larger batch size accelerates training but requires more data points to be visited per iteration [51]. Smaller batch sizes introduce a degree of stochastic noise into the gradient estimate; this very noise, however, exerts a regularizing influence on the fitted model and gives rise to a learning trajectory that is rapid yet fluctuating, characterized by elevated variance. Conversely, larger batch sizes temper the pace of learning but steer the optimization toward a more stable basin of convergence marked by diminished

© 2026 The Author(s). | Published by Institute of Smart Energy Systems Press

variance. The research literature recommends using larger batch sizes to foster a stable training regime whenever the requisite hardware resources are available, provided the batch size remains within the memory constraints of the GPU or CPU performing the computation. For conventional systems that do not benefit from GPU acceleration, smaller batch sizes—around 64 or 128—are advised. In accordance with these considerations, a batch size of 128 data points was settled upon for training the networks. The entire suite of data preprocessing tasks, descriptive data analysis routines, and model development and training workflows was implemented in a Python environment, using the Pandas, Keras, Scikit-learn, and Matplotlib libraries.

**Table 3.** Architecture of the deep neural networks.

| Layer | Type | Output shape | Activation function |
|---|---|---|---|
| 1 | Dense_1 | (None, 100) | tanh |
| 2 | Dropout | (dropout rate of 0.1) | - |
| 3 | Dense_2 | (None, 50) | ReLU |
| 4 | Dense_3 | (None, 20) | ReLU |
| 5 | Dense_4 | (None, 1) | linear |

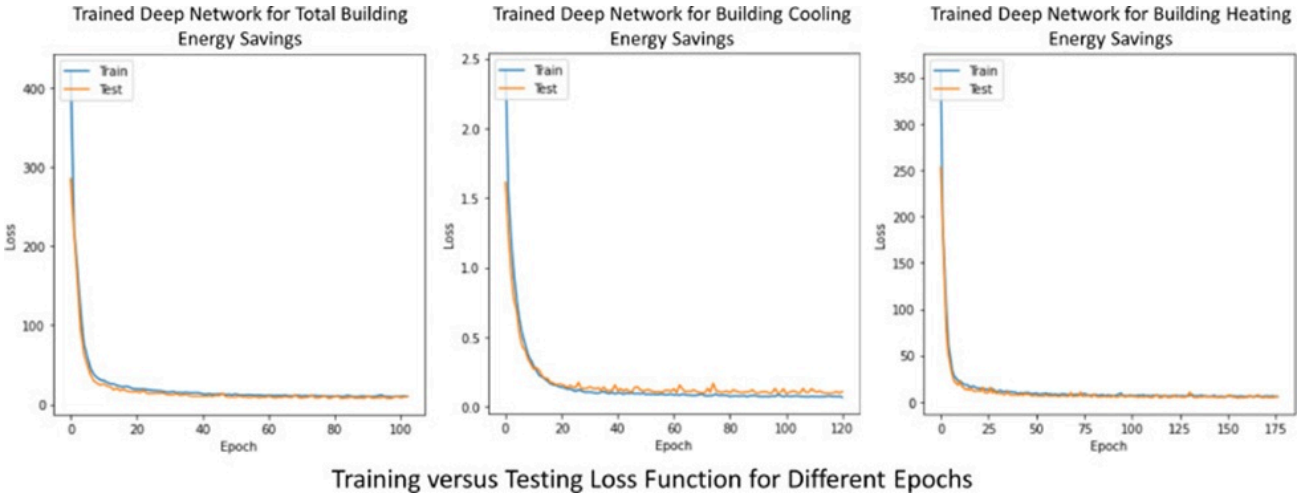



**Figure 5.** Training loss versus testing loss for different epoch numbers.

# Results and Discussion

## Descriptive statistics

This segment presents the outcomes of the descriptive statistical analysis applied to simulation-generated data, which capture the energy savings delivered by two competing facade systems as computed via building performance simulations. **Figure 6** depicts the frequency distributions of several salient predictor variables. Inspection of the figure reveals that all variables, with the singular exception of occupancy level, exhibit a wide spread of values. This property bolsters their capacity to explain variation in the target quantities (i.e., building energy savings). Among the dataset's attributes are two categorical variables: heating system category and cooling system category. A Spearman correlation analysis was subsequently performed to assess the monotonic relationship between these categorical inputs and the

© 2026 The Author(s). | Published by Institute of Smart Energy Systems Press

three energy savings targets—heat, cooling, and total site savings. As **Table 4** indicates, neither categorical variable demonstrates a notably strong correlation with any of the savings measures. Nonetheless, heating system type shows a marginally stronger correlation with building energy savings than does cooling system type. A caveat worth emphasizing is that the present analysis confined its scope to linear monotonic associations; it remains possible that non-linear dependencies linking the predictor features to the target variables also exist within the data.

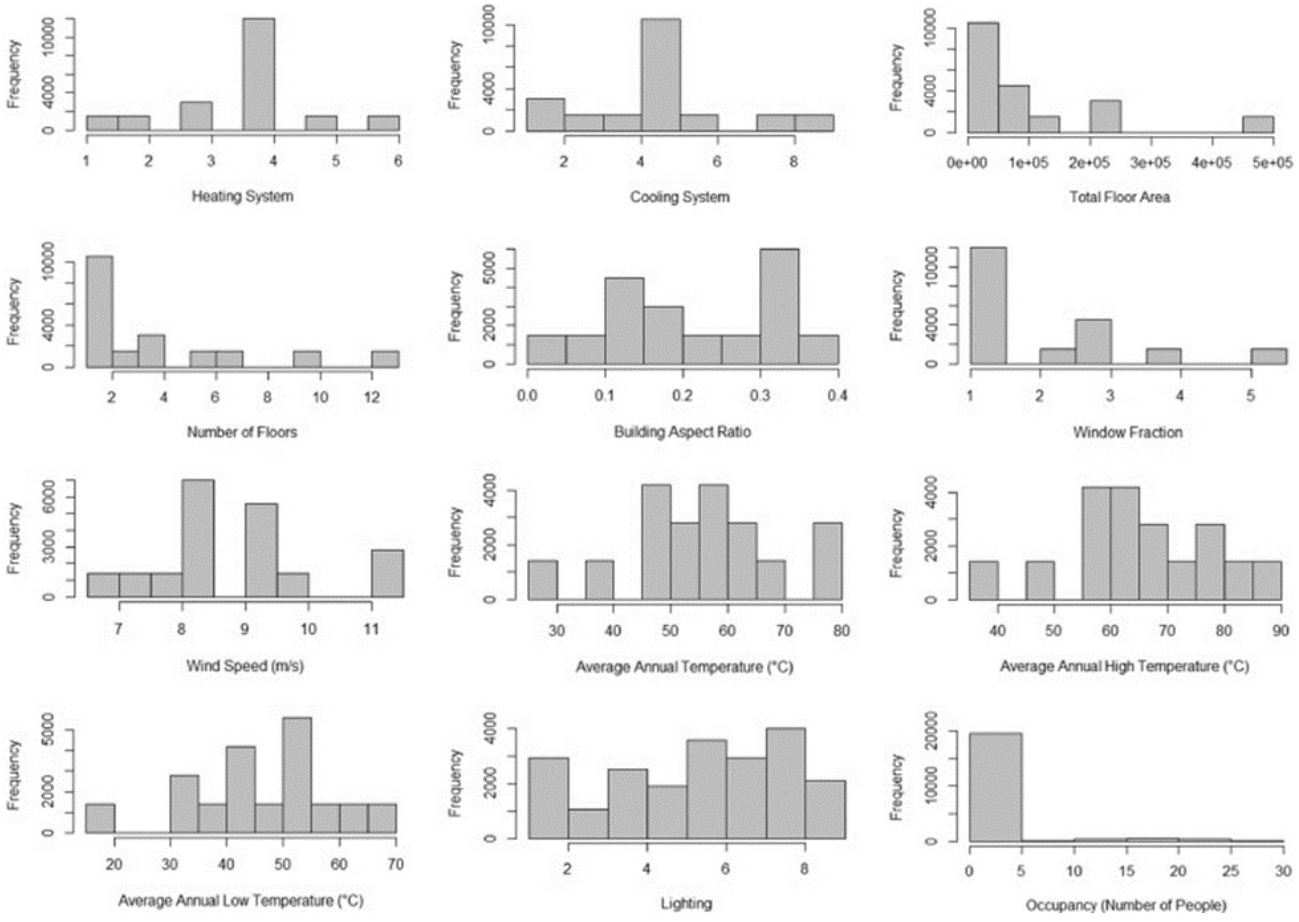



**Figure 6.** Frequency distribution of important input features.

**Table 4.** Spearman correlation between categorical features and building energy savings.

| Input variable | Heating energy savings (correlation) | Heating energy savings (P-value) | Cooling energy savings (correlation) | Cooling energy savings (P-value) | Total site energy savings (correlation) | Total site energy savings (P-value) |
|---|---|---|---|---|---|---|
| Space heating system | 0.186 | 5.21e-151 | 0.203 | 5.54e-180 | 0.247 | 5.46e-270 |
| Space cooling system | 0.127 | 1.58e-70 | 0.143 | 7.02e-90 | 0.173 | 3.71e-131 |

© 2026 The Author(s). | Published by Institute of Smart Energy Systems Press

Pearson's correlation analysis was next applied to the numerical features in the dataset, encompassing both building physical characteristics and weather-related parameters. **Figure 7** shows the Pearson correlation coefficients computed between building physical descriptors and the three building energy-saving measures. The pattern that emerges points to an inverse association between total site-building energy savings and a suite of physical building attributes—specifically, total floor area, building aspect ratio, floor count, window fraction, and lighting loads—with occupancy level alone breaking this trend. The strongest inverse relationship detected is between total site energy savings and floor count, meaning that a building with more stories tends to register lower total site energy savings.

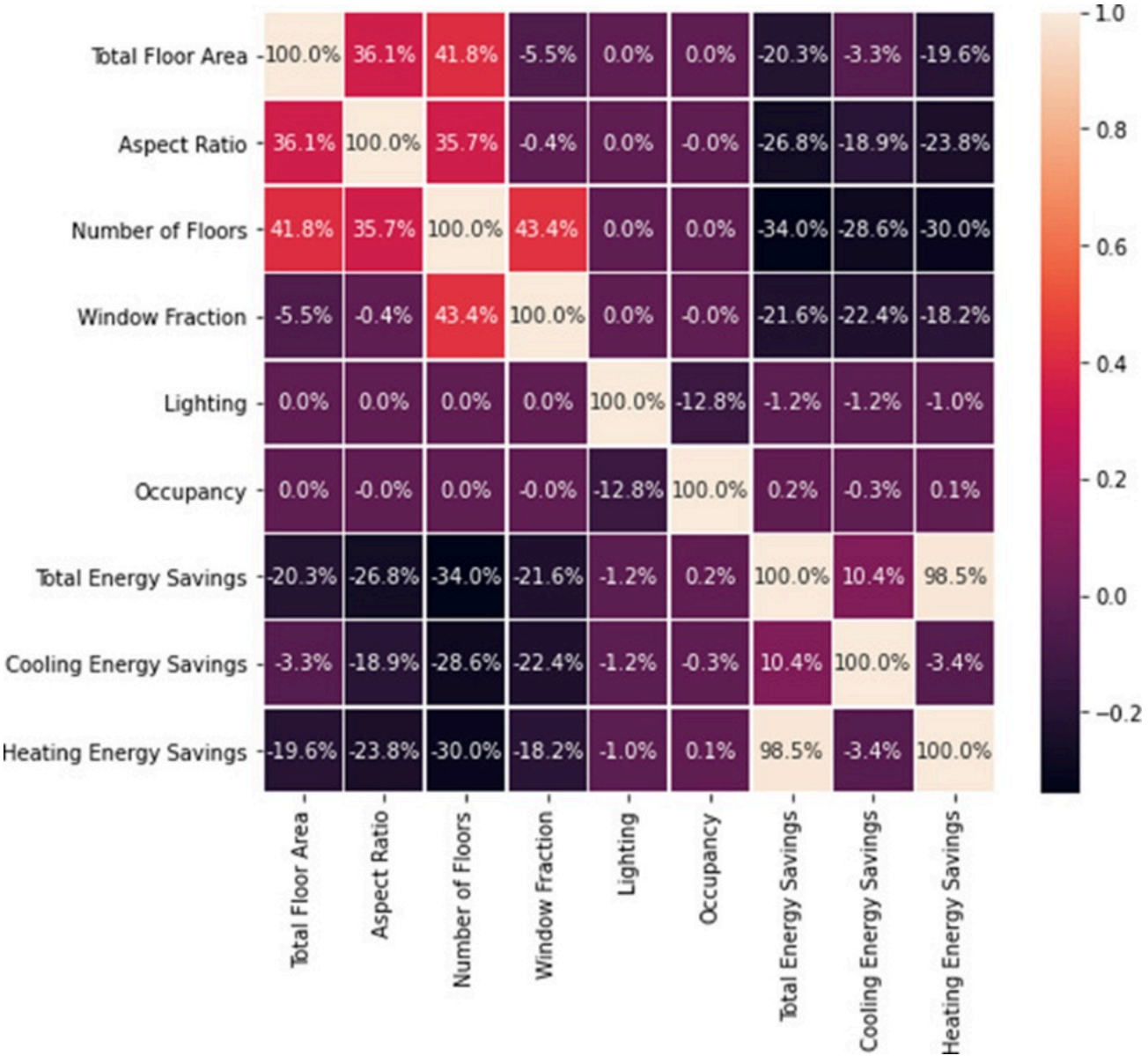



**Figure 7.** Pearson correlation between building physical characteristics and building energy savings.

In contrast, growth in the occupant population is accompanied by an uptick in total site energy savings. A parallel structure emerges when examining heating energy savings: the correlations with building physical features are all negative, with only occupancy level displaying the opposite sign. Extending this inquiry to cooling energy savings yields a broadly consistent picture, albeit with a notable distinction—cooling energy savings are negatively correlated with occupancy level. The practical implication of this finding is that a larger occupant count tends to depress cooling energy

© 2026 The Author(s). | Published by Institute of Smart Energy Systems Press

savings. The causal mechanism underlying this negative relationship lies in the metabolic heat output of human bodies, which directly increases the cooling load on the building's HVAC system.

**Figure 8** shifts the focus to the relationships between weather-related features and building energy savings. The data reveal robust positive correlations linking both total site energy savings and heating energy savings with the annual extremes and averages of ambient temperature—namely, the annual high, low, and mean temperature values. The implication is that upward movement in any of these temperature indicators will swell the total site energy savings and heating energy savings realized by a building finished with UHP-FRC panels relative to its counterpart equipped with conventional panels. Positive associations with wind speed are also apparent. At the opposite end of the spectrum, cooling energy savings display a strong negative correlation with annual high, low, and average temperatures, such that higher temperatures contract cooling energy savings. Notably, the correlations between wind speed metrics and cooling energy savings are stronger than those involving total and heating energy savings, suggesting that wind speed exerts a disproportionately large impact on cooling energy savings.

© 2026 The Author(s). | Published by Institute of Smart Energy Systems Press

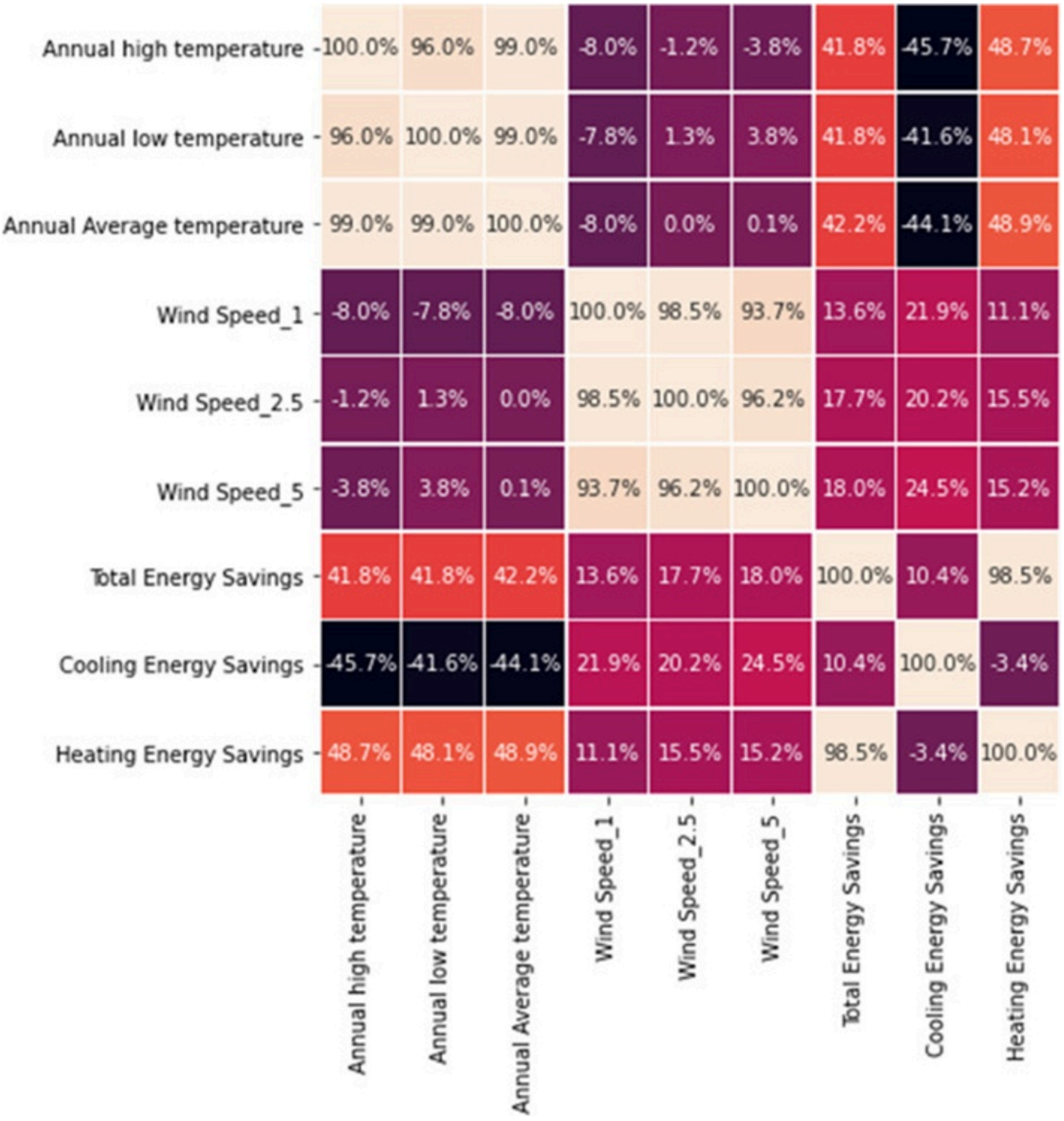



**Figure 8.** Pearson correlation between weather-related features and building energy savings.

**Figure 9** extends this correlational lens to monthly high and low temperature readings and their link to building energy savings. The evidence from this analysis suggests that weather-related features carry a stronger correlation with building energy savings than do building physical characteristics. Throughout the calendar, total site energy savings and heating energy savings maintain positive correlations with both monthly high and monthly low temperatures. In contrast, the correlational sign reverses for cooling energy savings, which are negatively associated with monthly high and low temperatures. An increase in temperature reduces the building's heating load but increases its cooling burden. This dynamic shifts month by month. During the winter months—exemplified by December and January—the cooling load drops to its annual trough, and cooling energy savings diminish accordingly; concurrently, the heating load escalates, yielding a corresponding increase in heating energy savings.

© 2026 The Author(s). | Published by Institute of Smart Energy Systems Press

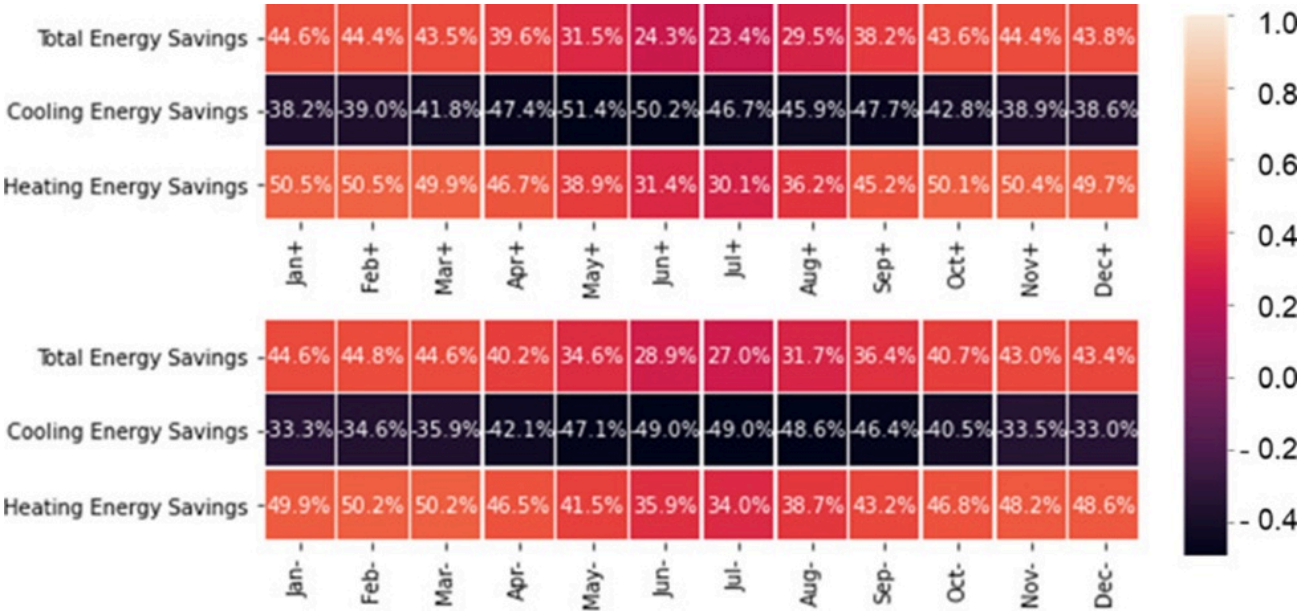



**Figure 9.** Pearson correlation between weather-related features and building energy savings.

## Prediction results

Three separate deep neural network models were devised and trained to estimate total site energy savings, cooling energy savings, and heating energy savings, respectively. Model performance was quantified on both the training and testing partitions using two standard metrics: mean absolute error (MAE) and root mean squared error (RMSE). **Table 5** records these evaluation statistics for each of the three networks. As the table shows, the network calibrated to project cooling energy savings achieved notably higher precision than the other two networks, a pattern that holds consistently across both the training and testing subsets. Furthermore, the gap between the training-set and testing-set performance is minimal in all three cases, providing clear evidence that the networks have achieved strong generalization and do not suffer from overfitting.

**Table 5.** Accuracy metrics of deep networks on training and testing datasets.

| Prediction target (neural networks) | Training MAE | Training RMSE | Testing MAE | Testing RMSE |
|---|---|---|---|---|
| Total site energy savings | 1.45 | 3.24 | 1.59 | 3.48 |
| Cooling energy savings | 0.17 | 0.30 | 0.20 | 0.39 |
| Heating energy savings | 1.01 | 2.38 | 1.17 | 2.72 |

## Feature importance

Feature importance extraction comprises a family of techniques that assign a numerical score to each predictor variable, reflecting its utility for forecasting the target. The operational logic is straightforward: feature importance is determined by tracking how much the model's predictive error increases after the feature's values are randomly permuted. A variable qualifies as "important" if scrambling its values provokes a sizable jump in model error; conversely, a variable is deemed "unimportant" if random rearrangement of its values produces virtually no change in model error [52, 53].

© 2026 The Author(s). | Published by Institute of Smart Energy Systems Press

The permutation-based feature importance method was employed to assess the relative contribution of each independent variable toward the estimation of building energy savings. **Figure 10** presents the ranked importance scores of the explanatory features across the three savings prediction tasks. Several attributes consistently emerge among those exerting the greatest influence on all three targets: total floor area, number of floors, annual high, low, and average ambient temperature readings, and the concrete density of the panel's structural wythe. These observations are consistent with the correlational patterns reported in the earlier section. For example, the correlation analysis previously indicated that the linear association between building occupancy level and energy savings is extremely weak. In a similar vein, **Figure 5** suggests that varying the occupancy level is unlikely to materially alter the energy savings values. On the other hand, the correlation analysis also indicated, as shown in **Figure 5**, that the annual high, low, and mean temperature measures, along with total floor area, show moderate correlations with energy savings.

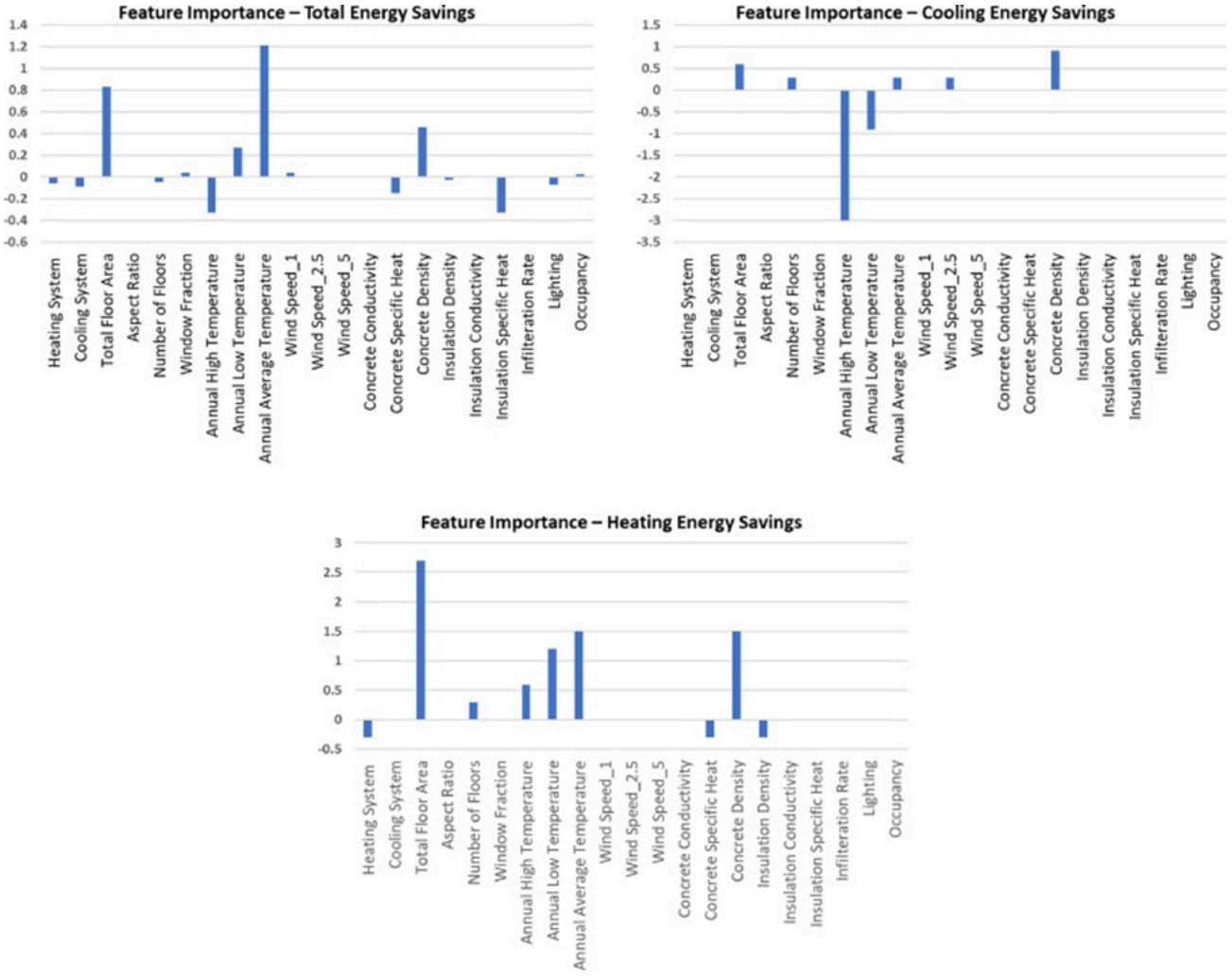



**Figure 10.** The relative importance of predictive features for deep networks.

## Comparison between deep neural networks and shallow neural networks, GBM, RF, and GLM

The generalization accuracy of deep neural networks was compared with that of a simple ANN architecture and three established data-driven modeling paradigms: Gradient Boosting Machine (GBM), Random Forest (RF), and the

© 2026 The Author(s). | Published by Institute of Smart Energy Systems Press

Generalized Linear Model (GLM).

Three shallow neural network models were developed to predict total site, cooling, and heating energy savings for buildings. The model designed for total site energy savings prediction consisted of an input layer, one fully connected hidden layer equipped with 100 hidden nodes, and an output layer. Training was performed over 113 iterations with a learning rate of 0.01. An identical structural configuration was reproduced for the networks intended to project cooling and heating energy savings. Convergence for the cooling energy savings model was reached at 145 iterations with a learning rate of 0.01. In contrast, the heating energy savings model completed training after 110 iterations at the same learning rate. Across all shallow networks, cross-entropy was adopted as the loss function.

Three GBM-based models were also trained on the total site, cooling, and heating energy savings tasks. The hyperparameter specification was kept uniform across all three: 270 trees (i.e., boosting rounds), a learning rate of 0.25, 32 leaves per tree, and a minimum of 6 observations per leaf. Similarly, three Random Forest models were constructed for the same three energy savings outputs, again using a consistent set of hyperparameters throughout. Each Random Forest model comprised 30 individual decision trees, capped at a maximum depth of 53, with 132 random split candidates evaluated at each node and a requirement of at least 2 samples to form a leaf node. Finally, three generalized linear regression models were specified, each regularized with an L2 penalty term with a weight of 0.001.

**Table 6** summarizes the testing-set predictive accuracy of every model—expressed via MAE and RMSE—across the total site, cooling, and heating energy savings prediction tasks. The comparative results unanimously point to the superior performance of deep neural networks in estimating building energy savings. The deep network trained to forecast total site energy savings achieved the most favorable accuracy (i.e., the smallest error) among all evaluated models, with a mean absolute error of 1.59 and a root mean square error of 3.48, ahead of GBM, followed by RF, and with GLM ranking last. Consistent with this outcome, the deep network targeting cooling energy savings achieved the lowest MAE of 0.20, followed by GBM, RF, and GLM, in that order. To complete the picture, the deep network developed for heating energy-savings predictions achieved the lowest MAE of 1.17 when compared with all alternative models. In summary, the testing metrics clearly show that deep neural networks outperform the competing modeling strategies examined here.

**Table 6.** Testing accuracy metrics of Deep Neural Networks, Shallow Neural Networks, GBM, Random Forest, and GLR models.

| Modeling approach | Prediction target | MAE | RMSE |
|---|---|---|---|
| Deep Neural Network | Total Site Energy Savings | 1.59 | 3.48 |
| | Cooling Energy Savings | 0.20 | 0.39 |
| | Heating Energy Savings | 1.17 | 2.72 |
| Shallow Neural Network | Total Site Energy Savings | 6.80 | 10.79 |
| | Cooling Energy Savings | 0.51 | 0.96 |
| | Heating Energy Savings | 5.70 | 10.16 |
| Gradient Boosting Machine | Total Site Energy Savings | 1.85 | 3.57 |
| | Cooling Energy Savings | 0.21 | 0.50 |
| | Heating Energy Savings | 1.44 | 3.08 |
| Random Forest | Total Site Energy Savings | 3.85 | 7.74 |
| | Cooling Energy Savings | 0.40 | 0.95 |

© 2026 The Author(s). | Published by Institute of Smart Energy Systems Press

| | | | |
|---|---|---|---|
| | Heating Energy Savings | 3.09 | 6.99 |
| Generalized Linear Model | Total Site Energy Savings | 9.20 | 14.47 |
| | Cooling Energy Savings | 0.98 | 1.58 |
| | Heating Energy Savings | 8.69 | 15.08 |

# Conclusion

This research set out to determine whether deep learning can be effectively applied to the appraisal of building facade systems at the preliminary design phase. A comprehensive campaign of 19,600 building performance simulations was undertaken to document the energy behavior of two contrasting facade technologies—Ultra-High-Performance Fiber-Reinforced-Concrete panels and conventional panels—under a range of climatic conditions and building archetypes. The resulting simulation corpus was used to train a set of deep neural networks to predict the energy savings associated with alternative facade designs. The predictive outputs of the deep neural networks were subsequently compared with those generated by several widely adopted predictive models (Gradient Boosting Machine, Random Forest, and Generalized Linear Regression) and with shallow neural network baselines. The comparative evaluation demonstrated that deep neural networks consistently deliver superior predictive accuracy compared to other models, thereby confirming the distinctive benefits of deep learning for early-stage screening of facade alternatives. The relative influence of the explanatory variables on the predictions was also extracted from the fitted deep neural networks. Six features were found to contribute disproportionately to the predictive outcomes: total floor area, number of floors, annual high, low, and average ambient temperature values, and the concrete density characterizing the panel's structural layer.

These findings underscore the promise of deep neural networks for enabling performance-driven assessment of competing facade concepts at the earliest moments of the building design trajectory. The methodological framework advanced here can be deployed as a decision-support instrument in early-stage facade design, helping practitioners move toward high-performance building solutions by providing preliminary estimates of the energy savings achievable with different facade configurations. Designers can draw upon this approach to acquire sufficient insight at the formative design stage, laying the foundation for well-informed decision-making. The framework put forward constitutes a generalizable structure that lends itself to expansion with additional predictor and response variables—for instance, occupant behavior and activity profiles or building energy consumption broken down by month. Nevertheless, several limitations constrain the present framework:

• The framework has been constructed around annualized building energy savings. Future investigations should aim to recalibrate the framework for finer temporal granularity, such as daily, weekly, or monthly savings data. Obtaining more finely resolved records from building energy simulations would enable the training of sequence-based architectures, including recurrent neural networks, to model the temporal dynamics of building energy savings.

• The framework, as currently formulated, is oriented toward offering recommendations for adopting a specific facade panel over a baseline panel under diverse circumstances. Subsequent studies should extend the framework to incorporate, as baseline comparators, the energy performance benchmarks prescribed by established building energy efficiency codes—such as those issued by the American Society of Heating, Refrigerating and Air-Conditioning Engineers or the International Energy Conservation Code.

# Acknowledgements

None

© 2026 The Author(s). | Published by Institute of Smart Energy Systems Press

# Conflict of interest

None

# Financial support

None

# Ethics statement

None

Received: 06 Nov 2024 Revised: 12 Jan 2025 Accepted: 30 Jan 2025
Published online: 15 June 2026

## Rights and permissions

**Open Access** The author(s) retain copyright. This article is licensed under the Creative Commons Attribution-NonCommercial-ShareAlike 4.0 International License. It may be shared and adapted for non-commercial purposes with appropriate attribution, an indication of changes, and distribution of adaptations under the same license. Third-party material may be subject to separate terms identified in its credit line. View the license at https://creativecommons.org/licenses/by-nc-sa/4.0/.

# References

1. U.S. Energy Information Administration. How much energy is consumed in U.S. buildings? [Internet]. 2020 Dec 22 [cited 2026 Jul 8]. Available from: https://www.eia.gov/tools/faqs/faq.php?id=86&t=1

2. U.S. Energy Information Administration. How much energy is consumed in U.S. buildings? [Internet]. Washington, DC: U.S. Energy Information Administration; 2020 [cited 2026 Aug 19]. Available from: https://www.eia.gov/tools/faqs/faq.php?id=86&t=1

3. Amiri SS, Mottahedi M, Asadi S. Using multiple regression analysis to develop energy consumption indicators for commercial buildings in the US. Energy Build. 2015;109:209-16.

4. Asadi S, Amiri SS, Mottahedi M. On the development of multi-linear regression analysis to assess energy consumption in the early stages of building design. Energy Build. 2014;85:246-55.

5. Hari A. Integrated, customer driven, conceptual design methodology [doctoral dissertation]. Haifa (Israel): Technion, Israel Institute of Technology; 2001. 265 p. Hebrew.

6. Abediniangerabi B. Assembly-scale and whole-building energy performance analysis of ultra-high-performance fiber-reinforced concrete (UHP-FRC) façade systems [doctoral dissertation]. Arlington (TX): University of Texas at Arlington; 2019.

7. Zhao HX, Magoulès F. A review on the prediction of building energy consumption. Renew Sustain Energy Rev. 2012;16(6):3586-92.

8. Abediniangerabi B, Shahandashti SM, Makhmalbaf A. A data-driven framework for energy-conscious design of building facade systems. J Build Eng. 2020;29:101172.

9. Pannu A. Artificial intelligence and its application in different areas. Artif Intell. 2015;4(10):79-84.

10. Wang Z, Srinivasan RS. A review of artificial intelligence based building energy use prediction: contrasting the capabilities of single and ensemble prediction models. Renew Sustain Energy Rev. 2017;75:796-808.

11. Ashouri M, Haghighat F, Fung BC, Lazrak A, Yoshino H. Development of building energy saving advisory: a data mining approach. Energy Build. 2018;172:139-51.

12. Sun Y, Haghighat F, Fung BC. A review of the-state-of-the-art in data-driven approaches for building energy prediction. Energy Build. 2020;110022.

13. Zeng A, Ho H, Yu Y. Prediction of building electricity usage using Gaussian Process Regression. J Build Eng. 2020;28:101054.

14. Wu J, Lian Z, Zheng Z, Zhang H. A method to evaluate building energy consumption based on energy use index of different functional sectors. Sustain Cities Soc. 2020;53:101893.

15. Yu Z, Haghighat F, Fung BC, Yoshino H. A decision tree method for building energy demand modeling. Energy Build. 2010;42(10):1637-46.

16. Fan C, Xiao F, Wang S. Development of prediction models for next-day building energy consumption and peak power demand using data mining techniques. Appl Energy. 2014;127:1-10.

17. Gassar AAA, Cha SH. Energy prediction techniques for large-scale buildings towards a sustainable built environment: a review. Energy Build. 2020;110238.

18. Pham AD, Ngo NT, Truong TTH, Huynh NT, Truong NS. Predicting energy consumption in multiple buildings using machine learning for improving energy efficiency and sustainability. J Clean Prod. 2020;121082.

19. Touzani S, Granderson J, Fernandes S. Gradient boosting machine for modeling the energy consumption of commercial buildings. Energy Build. 2018;158:1533-43.

20. Montgomery JM, Olivella S. Tree-based models for political science data. Am J Polit Sci. 2018;62(3):729-44.

21. Chang LY, Chen WC. Data mining of tree-based models to analyze freeway accident frequency. J Safety Res. 2005;36(4):365-75.

22. Singh P, Dwivedi P. Integration of new evolutionary approach with artificial neural network for solving short term load forecast problem. Appl Energy. 2018;217:537-49.

23. Ahmad AS, Hassan MY, Abdullah MP, Rahman HA, Hussin F, Abdullah H, et al. A review on applications of ANN and SVM for building electrical energy consumption forecasting. Renew Sustain Energy Rev. 2014;33:102-9.

24. Melo AP, Cóstola D, Lamberts R, Hensen JLM. Development of surrogate models using artificial neural network for building shell energy labelling. Energy Policy. 2014;69:457-66.

25. Rahman A, Smith AD. Predicting fuel consumption for commercial buildings with machine learning algorithms. Energy Build. 2017;152:341-58.

26. Jiang Y, Bosch N, Baker RS, Paquette L, Ocumpaugh J, Andres JMA, et al. Expert feature-engineering vs. deep neural networks: which is better for sensor-free affect detection? In: Proceedings of the International Conference on Artificial Intelligence in Education. Cham: Springer; 2018. p. 198-211.

27. Abediniangerabi B, Shahandashti SM. Hygrothermal investigation of facade panel connections using a transient coupled heat and moisture transport model. In: COMSOL Conference 2020 – North America; 2020.

© 2026 The Author(s). | Published by Institute of Smart Energy Systems Press

28. Abediniangerabi B, Shahandashti M, Makhmalbaf A. Coupled transient heat and moisture transfer investigation of facade panel connections. J Eng Des Technol. 2020.

29. Abediniangerabi B, Shahandashti SM, Bell B, Chao SH, Makhmalbaf A. Building energy performance analysis of ultra-high-performance fiber-reinforced concrete (UHP-FRC) façade systems. Energy Build. 2018;174:262-75.

30. U.S. Department of Energy. Energy Efficiency & Renewable Energy Office Commercial Prototype Building Models [Internet]. 2018 [cited 2026 Jul 8]. Available from: https://www.energycodes.gov/development/commercial/prototype_models

31. Abediniangerabi B, Shahandashti SM, Bell B, Chao SH, Makhmalbaf A. Assembly-scale and whole-building energy performance analysis of ultra-high-performance fiber-reinforced concrete (UHP-FRC) Façade systems. In: 2nd International Interactive Symposium on UHPC; 2019 Jun 2-5; Albany, NY.

32. Li Q, Gu L, Augenbroe G, Wu C, Brown J. A generic approach to calibrate building energy models under uncertainty using Bayesian Inference. In: BS2015: 14th Conference of International Building Performance Simulation Association; 2015 Dec 7-9; Hyderabad, India. p. 2913-22.

33. Menberg K, Heo Y, Augenbroe G, Choudhary R. New extension of Morris method for sensitivity analysis of building energy models. In: Build Simul Optim; 2016.

34. Robati M, Daly D, Kokogiannakis G. A method of uncertainty analysis for whole-life embodied carbon emissions (CO2-e) of building materials of a net-zero energy building in Australia. J Clean Prod. 2019;225:541-53.

35. Shahandashti SM, Abediniangerabi B, Bell B, Chao SH. [Unpublished work]. 2017.

36. McKay MD, Beckman RJ, Conover WJ. A comparison of three methods for selecting values of input variables in the analysis of output from a computer code. Technometrics. 2000;42(1):55-61.

37. Macdonald IA. Quantifying the effects of uncertainty in building simulation [doctoral dissertation]. Glasgow (UK): University of Strathclyde; 2002.

38. U.S. Department of Energy. [Internet]. 2020 [cited 2026 Jul 8]. Available from: https://www.energy.gov/

39. Bhamornsiri C, Gomez P, Wilson T, Eisenhower B. Calibration of envelope parameters using control-based heat balance identification and uncertainty analysis. In: Proceedings of BS2013: 13th Conference of International Building Performance Simulation Association; 2013 Aug 26-28; Chambéry, France.

40. Dhariwal J, Banerjee R. Naturally ventilated building design under uncertainty using design of experiments. In: Building Simulation Conference; 2015. p. 1708-15.

41. Hopfe C, Hensen J, Plokker W. Uncertainty and sensitivity analysis for detailed design support. In: Proceedings of the 10th IBPSA Building Simulation Conference; 2007 Sept 3-6; Tsinghua University, Beijing, China. p. 3-5.

42. Lee BD, Sun Y, Augenbroe G, Paredis CJ. Towards better prediction of building performance: a workbench to analyze uncertainty in building simulation. In: 13th International Building Performance Simulation Association Conference; 2013 Aug 26-28; Chambéry, France.

43. Lomas KJ, Eppel H. Sensitivity analysis techniques for building thermal analysis simulation program. Energy Build. 1992;19(1):21-44.

44. Petr K, Filip J, Karel K, Jan H. Technique of uncertainty and sensitivity analysis for sustainable building energy systems performance calculations. In: Proceedings of the 10th Conference of International Building Performance Simulation Association; 2007 Sept 3-6; Tsinghua University, Beijing, China. p. 629-36.

© 2026 The Author(s). | Published by Institute of Smart Energy Systems Press

45. Soto AM, Jentsch MF. Sensitivity and uncertainty analysis of models for determining energy consumption in the residential sector. In: Proceedings of BS2015: 14th Conference of International Building Performance Simulation Association; 2015 Dec 7-9; Hyderabad, India.

46. Graves A. Supervised sequence labelling. In: Supervised sequence labelling with recurrent neural networks. Berlin, Heidelberg: Springer; 2012. p. 5-13.

47. McCulloch WS, Pitts W. A logical calculus of the ideas immanent in nervous activity. Bull Math Biophys. 1943;5(4):115-33.

48. Rumelhart DE, Hinton GE, Williams RJ. Learning internal representations by error propagation (No. ICS-8506). La Jolla (CA): California Univ San Diego Inst for Cognitive Science; 1985.

49. LeCun Y, Bengio Y, Hinton G. Deep learning. Nature. 2015;521(7553):436-44.

50. Hemdan EED, Shouman MA, Karar ME. Covidx-net: a framework of deep learning classifiers to diagnose covid-19 in x-ray images [preprint]. arXiv:2003.11055. 2020.

51. Bengio Y. Practical recommendations for gradient-based training of deep architectures. In: Neural networks: Tricks of the trade. Berlin, Heidelberg: Springer; 2012. p. 437-78.

52. Breiman L. Random forests. Mach Learn. 2001;45(1):5-32.

53. Fisher A, Rudin C, Dominici F. All models are wrong, but many are useful: learning a variable's importance by studying an entire class of prediction models simultaneously. J Mach Learn Res. 2019;20(177):1-81.

© 2026 The Author(s). | Published by Institute of Smart Energy Systems Press